

Simultaneous analysis of photoinduced electron transfer in wild type and mutated AppAs

Nadtanet Nunthaboot^a, Fumio Tanaka^{a,*}, Sirirat Kokpol^b

^a Department of Chemistry, Faculty of Science, Mahasarakham University, Mahasarakham 44150, Thailand

^b Department of Chemistry, Faculty of Science, Chulalongkorn University, Bangkok 10330, Thailand

ARTICLE INFO

Article history:

Received 1 August 2009

Received in revised form 13 October 2009

Accepted 31 October 2009

Available online 6 November 2009

Keywords:

Photoinduced electron transfer

Fluorescence dynamics

Flavin photoreceptor

BLUF

AppA

Mutated AppA

Kakitani and Mataga electron transfer theory

ABSTRACT

Photoinduced electron transfer (PET) from Tyr21 to isalloxazine (Iso) in the excited state (Iso*) is considered to be an initial step of the photosensing function of the blue-light sensing using flavin adenine dinucleotide (BLUF) component of the anti-repressor of the photosynthetic regulation (AppA). The PET mechanism was investigated via fluorescence dynamics of AppA and Kakitani and Mataga (KM) theories as well as by molecular dynamic (MD) simulation. The local structures of both the Y21F and W104F mutant AppAs around the Iso binding sites were quite different from those of the wild type (WT) AppA. The distances between Iso and Trp104 in Y21F, and between Iso and Tyr21 in W104F were shorter by 0.06 nm and 0.02 nm, respectively, compared to the WT. The frequency factor, ν_0 , in Tyr21 was 1.15-fold greater than that in Trp104. The critical distance between adiabatic and non-adiabatic PET processes, R_0 , was found to be very long in the AppA Tyr21. The large values of ν_0 and R_0 for Tyr21 of AppA compared to those in a non photosensing flavoprotein, FMN binding protein (FBP), were elucidated by hydrogen bond (H bond) chain between Tyr21 and Iso through Gln63. Interaction energies among Iso*, Trp104, Tyr21 and Gln63 in WT were calculated using the semi-empirical PM3 method. The amount of the transferred charge from Trp104 to Iso* in the WT exhibited a maximum at an interaction energy of around -20 kcal/mol, but decreased as the interaction energy (absolute value) increased.

© 2009 Elsevier B.V. All rights reserved.

1. Introduction

The anti-repressor of the photosynthetic gene expression regulon (AppA) in the purple bacterium of *Rhodobacter sphaeroides* [1–10], contains two domains, a Cys-rich carboxyl-terminal domain that is responsible for the isomerization of a disulfide bond in the photosynthetic repressor (PpsR) of this regulon, and an amino terminal domain that non-covalently binds with the blue-light sensing using FAD (BLUF) [1]. AppA also contains non-covalently bound heme in its central part [3]. The heme dissociates with increasing O₂ concentrations, which correlates well with the observed decrease in transcription of photosynthesis genes from this regulon [3]. The entire AppA undergoes a photocycle with blue-light irradiation, which brings about a signaling state of flavin with a long-lived 10 nm red-shift in the absorption spectrum [1]. Without Tyr21, the BLUF component of AppA does not function as a photosensor and this particular residue, therefore, is considered to play an essential role in AppA photosensing [2,3]. It was also demonstrated by Fourier transformed infrared spectroscopy (FTIR) based analysis that hydrogen-bonding rearrangements between

isalloxazine (Iso) and nearby amino acids takes place and relatively large structural changes occur in the protein backbone of the AppA BLUF upon illumination [5]. Photoinduced electron transfer (PET) in the wild type (WT) [6,7] and Y21F [8] and W104F [9] mutant AppAs was investigated by means of fluorescence dynamics and transient absorption spectroscopy. In the WT AppA, the signaling state is formed from Iso* with lifetimes of 90 ps and 570 ps [6]. PET in the BLUF domain of Slr11694, as observed by ultrafast experiments [11], brings about the sequential formation of anionic Iso⁻ and neutral IsoH on a picosecond time scale. Structures of the dark state [4,12] and the signaling state [12] of AppA were determined by X-ray diffraction (XRD). The photophysics of AppA in the signaling state were also investigated by means of a transient absorption spectroscopy [13]. Domracheva et al. [14] provided a quantum mechanical basis for the photoinduced tautomerization of the AppA Gln63 residue accompanied by PET from Tyr21 to Iso* through Gln63 with H bonds. Regarding light absorption by AppA in the signaling state, Iso* decayed mono-exponentially with a 7 ps lifetime to form the neutral IsoH, which subsequently decayed to the original Iso in the ground state within 60 ps [13]. Recently, BLUF from sources other than *R. sphaeroides* have also been characterized [11,14–21].

On the other hand, PET in non-photosensing flavoproteins has been systematically investigated by Mataga and co-workers

* Corresponding author. Tel.: +66 43 754246.

[22–29], where it has been demonstrated, by means of picosecond- [30,31] and femtosecond-resolved [32,33] transient absorption spectroscopy, that PET takes place from Trp and/or Tyr to Iso*. The donor–acceptor distance-dependent PET rates in these flavoproteins have been expressed with center-to-center distances rather than edge-to-edge distances [26], and the distance-dependence of PET rates was analyzed with three kinds of PET theory [27].

Various theories have been modeled for PET processes in bulk solution [34–42]. The ultrafast fluorescence dynamics of the WT, W32Y and W32A non-photosensory flavoproteins FBP were investigated by means of the up-conversion method [34]. The fluorescence decay of WT FBP [43] was analyzed using MD simulation coordinates and PET theories by Marcus and co-workers [34–36], Bixon and Jortner [37–39] and by Katitani and Mataga (KM) theories [40–42]. In the analysis, the electrostatic interaction energies between each of the Iso anion, Trp cations and Tyr cation with the other ionic groups were introduced into the PET theories. This greatly improved the agreement between the calculated and the observed [43] fluorescence decay rates. The fluorescence dynamics of WT, W32Y and W32A FBP were also simultaneously analyzed to determine the PET parameters contained within the KM theory [44], where PET parameters for Trp and Tyr were separately determined.

The PET in BLUF has never been analyzed with PET theory, yet it is very important to understand PET on the basis of PET theory. In the present work, we describe a theoretical basis for PET in AppA, simultaneously analyzing the reported fluorescence decays of the WT [6], and the Y21F [8] and W104F [9] mutant AppAs, with the atomic coordinates in Iso, Trp104 and Tyr21 obtained by MD and KM theory. The amount of transferred charge and the interaction energy in the Iso*–Trp104–Tyr21–Gln63 system was obtained by means of semi-empirical molecular orbital (MO) theory.

2. Methods of analyses

2.1. MD calculation

The starting structures of the two mutated AppA were obtained by modifying the X-ray structure of the wild type AppA (PDB code 1YRX) [4]. For Y21F and W104F, tyrosine at position 21 and tryptophan at position 104, respectively, were replaced by phenylalanine. These amino acid replacements were done using the Swiss PDB Viewer [50]. The LEap module of the Amber suit of programs [51] was used to prepare the simulated systems. Protein parameters were described by the parm99 force field [52], whilst force field parameters for Iso were taken from Schneider and Suhnel [53]. The two complexes were solvated in a box of 9777 TIP3P water molecules with approximate dimensions of 61 Å × 79 Å × 82 Å. To maintain the electroneutrality of each case, three Na⁺ counterions were added to neutralize the simulated systems. The added water molecules were first minimized and then the entire complex was completely relaxed over 1000 steps of steepest descent and 2000 steps of conjugate gradient. After minimization, each system was gradually heated from 10 to 298 K over 50 ps and was further equilibrated under the same temperature.

All calculations were carried out using the AMBER8 software package [51]. The system was set up under the isobaric–isothermal ensemble (NPT) with a constant pressure of 1 atm and a constant temperature of 298 K. Periodic boundary conditions were applied and the electrostatic interaction was corrected by the particle mesh Ewald method [54]. The SHAKE algorithm [55] was employed to constrain all bonds involving hydrogen atoms. A cutoff distance of 10 Å was employed for non-bonded pair interactions. MD calculations were performed with a relaxation time of 2 fs. All simulations were conducted over 3000 ps and production phase took from 1000 to 3000 ps with each snapshot collected every 0.01 ps.

2.2. PET theory

The PET rate by KM theory [40–42] was used for the fluorescence decay analysis. Details of KM theory are described in [Supplementary material A](#). The electrostatic interaction energy was incorporated into KM theory, as in previous works [43–45]. R_c (center to center distance) was used as the donor–acceptor distance [26,27]. The electrostatic energy in the WT AppA and its mutated proteins, Y21F and W104F, are also described in [Supplementary material A](#).

2.3. Observed and calculated fluorescence decays

The fluorescence decay functions of WT, Y21F and W104F were as reported [6,8,9], and are expressed by Eqs. (1)–(3), respectively.

$$F_{\text{obs}}^{\text{WT}}(t) = 0.10 \exp\left(-\frac{t}{25}\right) + 0.32 \exp\left(-\frac{t}{150}\right) + 0.56 \exp\left(-\frac{t}{670}\right) + 0.02 \exp\left(-\frac{t}{3800}\right) \quad (1)$$

$$F_{\text{obs}}^{\text{Y21F}}(t) = 0.17 \exp\left(-\frac{t}{7.5}\right) + 0.42 \exp\left(-\frac{t}{55}\right) + 0.40 \exp\left(-\frac{t}{212}\right) + 0.01 \exp\left(-\frac{t}{7100}\right) \quad (2)$$

$$F_{\text{obs}}^{\text{W104F}}(t) = 0.14 \exp\left(-\frac{t}{47}\right) + 0.63 \exp\left(-\frac{t}{555}\right) + 0.23 \exp\left(-\frac{t}{2500}\right) \quad (3)$$

where lifetimes are expressed in ps. The calculated decays [43–45] were expressed as Eqs. (4)–(6) for WT, W32Y and W32A, respectively.

$$F_{\text{calc}}^{\text{WT}}(t) = \left\langle \exp\{-k_{\text{ET}}^{\text{Trp104}}(t') + k_{\text{ET}}^{\text{Tyr21}}(t')\}t \right\rangle_{\text{AV}} \quad (4)$$

$$F_{\text{calc}}^{\text{Y21F}}(t) = \left\langle \exp\{-k_{\text{ET}}^{\text{Trp104}}(t')\}t \right\rangle_{\text{AV}} \quad (5)$$

$$F_{\text{calc}}^{\text{W104F}}(t) = \left\langle \exp\{-k_{\text{ET}}^{\text{Tyr21}}(t')\}t \right\rangle_{\text{AV}} \quad (6)$$

where $k_{\text{ET}}^{\text{Trp104}}(t')$, $k_{\text{ET}}^{\text{Tyr21}}(t')$ are the PET rates from Trp104 and Tyr21, respectively, to Iso*, which are given by Eq. (A1) in [Supplementary material A](#). $\langle \dots \rangle_{\text{AV}}$ means averaging procedure of the exponential function in Eqs. (4)–(6) over t' up to 2 ns at 0.1 ps time intervals. The time intervals of t in Eqs. (4)–(6) were all 1 ps. In Eqs. (4)–(6) we assumed that the decay functions during the MD time ranges can be always expressed by exponential functions at every instant of time, t' . Comparison between the present method and the one by Henry and Hochstrasser [57] is described in [Supplementary material B](#).

2.4. Determination of PET parameters

The unknown PET parameters contained in the KM theory, as listed in [Table 2](#), were determined to obtain the minimum

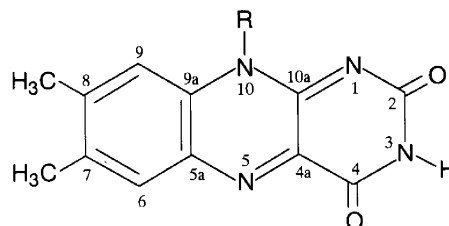


Chart 1. Chemical structure and atom notations of the Iso ring.

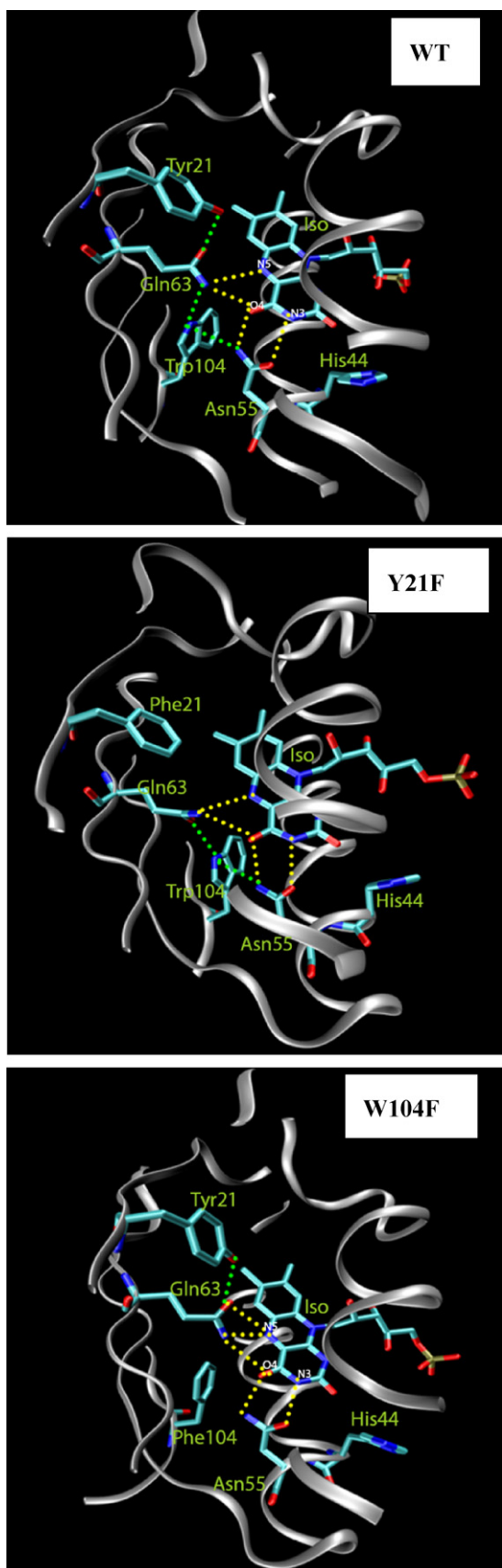


Fig. 1. Structures of WT, Y21F and W104F at Iso binding sites obtained by MD. H bonds with a distance of less than 0.35 nm of maximum distribution are indicated by yellow dots between Iso and the nearby amino acids, and by green dots between amino acids.

value of χ^2 , defined by Eq. (7), by means of a non-linear least squares method, according to the Marquadt algorithm, as previously reported [44–46].

$$\chi^2 = \frac{1}{N_{WT}} \sum_{i=1}^{N_{WT}} \frac{\{F_{\text{calc}}^{WT}(t_i) - F_{\text{obs}}^{WT}(t_i)\}^2}{F_{\text{calc}}^{WT}(t_i)} + \frac{1}{N_{Y21F}} \sum_{i=1}^{N_{Y21F}} \frac{\{F_{\text{calc}}^{Y21F}(t_i) - F_{\text{obs}}^{Y21F}(t_i)\}^2}{F_{\text{calc}}^{Y21F}(t_i)} + \frac{1}{N_{W104F}} \sum_{i=1}^{N_{W104F}} \frac{\{F_{\text{calc}}^{W104F}(t_i) - F_{\text{obs}}^{W104F}(t_i)\}^2}{F_{\text{calc}}^{W104F}(t_i)} \quad (7)$$

where N_{WT} , N_{Y21F} and N_{W104F} denote the numbers of time intervals of WT, Y21F and W104F, respectively. N_{WT} , N_{Y21F} and N_{W104F} were all 1250. Deviations between the observed and calculated intensities in WT, Y21F and W104F were expressed by Eqs. (8) – (10), respectively.

$$\text{Deviation(WT; } t_i) = \frac{\{F_{\text{calc}}^{WT}(t_i) - F_{\text{obs}}^{WT}(t_i)\}}{\sqrt{F_{\text{calc}}^{WT}(t_i)}} \quad (8)$$

$$\text{Deviation(Y21F; } t_i) = \frac{\{F_{\text{calc}}^{Y21F}(t_i) - F_{\text{obs}}^{Y21F}(t_i)\}}{\sqrt{F_{\text{calc}}^{Y21F}(t_i)}} \quad (9)$$

$$\text{Deviation(W104F; } t_i) = \frac{\{F_{\text{calc}}^{W104F}(t_i) - F_{\text{obs}}^{W104F}(t_i)\}}{\sqrt{F_{\text{calc}}^{W104F}(t_i)}} \quad (10)$$

2.5. MO calculation

The atomic coordinates of Iso, Trp104, Tyr21 and Gln63 were obtained from the MD data. Iso was substituted with lumiflavin, Trp104 with 3-methylindole, Tyr21 with 4-methylphenol and Gln63 with propanamide, respectively. The atomic coordinates of 40 MD structures were extracted from 20,000 MD structures with 50 ps time intervals up to 2 ns. MO calculations were performed with the WinMOPAC software package (Professional, Version 3.9; Fujitsu, Tokyo) [58]. The geometries of the Iso–Trp104–Tyr21–Gln63 system were optimized with the semi-empirical MO of PM3. Key words used for the MO calculations were EF (geometry optimized), PM3 (abbreviation of a semi-empirical MO method, Modified Neglect of Diatomic Overlap, Parametric Method 3), PRECISE (convergence condition is to be strict by 100 times), EXCITED (calculation is to be made to the first excited singlet state), XYZ (molecular structures are given by XYZ coordinates), GEO-OK (neglect of check for abnormal access between atoms) and EPS (solvent effect to the excited state is taken into account with conductor-like screening model). A more precise description of the PM3 parameters is given at <http://openmopac.net/>. The value of ϵ_0 (static dielectric constant) used was 24 [45]. Interaction energy (ΔE) among Iso*, Trp104, Tyr21 and Gln63 was evaluated by Eq. (11).

$$\Delta E = \Delta H_f(\text{Iso}^* - \text{Trp104} - \text{Tyr21} - \text{Gln63}) - \{ \Delta H_f(\text{Iso}^*) + \Delta H_f(\text{Trp104}) + \Delta H_f(\text{Tyr21}) + \Delta H_f(\text{Gln63}) \} \quad (11)$$

where $\Delta H_f(\text{Iso}^* - \text{Trp104} - \text{Tyr21} - \text{Gln63})$ denotes the heat of formation in the system of Iso*–Trp104–Tyr21–Gln63. $\Delta H_f(\text{Iso}^*)$, $\Delta H_f(\text{Trp104})$, $\Delta H_f(\text{Tyr21})$ and $\Delta H_f(\text{Gln63})$ are the heat of formation in the independent systems of Iso*, Trp104, Tyr21 and Gln63, respectively. The heat of formation contains the total electronic energy, the core-core repulsion energy between atoms and the heat of formation of all constituent atoms.

3. Results

3.1. MD structures of WT, Y21F and W104F at the Iso binding site

The chemical structure of Iso and atomistic notations are given in a Chart 1. The local structures of WT, Y21F and W104F at Iso binding sites obtained by MD are shown in Fig. 1. In these structures, H bonds between Iso and the nearby amino acids are indicated by yellow dots, and between amino acids by green dots. The time-dependent changes in the geometry around Iso in Y21F and W104F are shown in Fig. 2, and the numerical data of the geometry of the mutated AppAs are summarized in Table 1, together with those for the WT AppA for comparison. The mean center-to-center distances (R_c) between Iso and Trp104 in Y21F and between Tyr21 and Iso in W104F were by 0.06 and 0.02 nm, respectively, shorter than those in the WT. The distance between Iso and Trp64 was

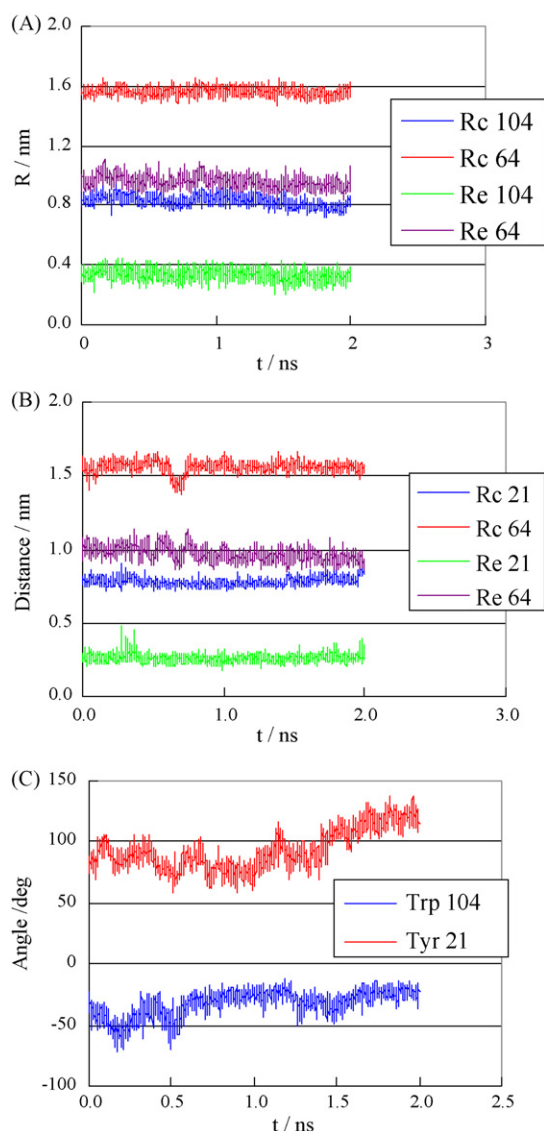


Fig. 2. Time-dependent changes in the geometry around Iso in the Y21F and W104F AppAs. (A) Distance between Iso and Trp104 or Trp64 in Y21F. Rc104 and Re104 denote the center-to-center (R_c) and edge-to-edge (R_e) distances between Iso and Trp104, respectively, whilst Rc64 and Re64 denote the same for Iso and Trp64. (B) Distance between Iso and Tyr21 or Trp64 in W104F. Rc21 and Re21 denote the center-to-center (R_c) and edge-to-edge (R_e) distances between Iso and Tyr21, respectively, whilst Rc64 and Re64 denote the same for Iso and Trp64. (C) Inter-ring angle between Iso and Trp104 in Y21F (Trp104), and between Iso and Tyr21 in W104F (Tyr21).

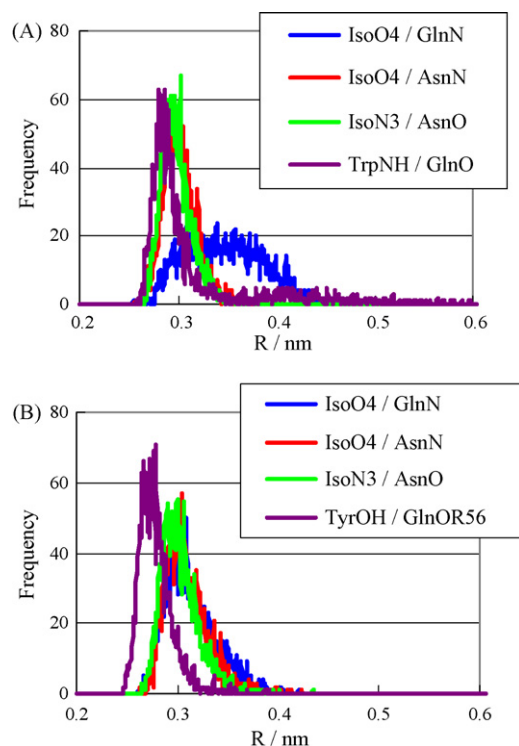


Fig. 3. Distribution frequency for the distances (R ; nm) between potential H bond pairs in AppA from (A) Y21F and (B) W104F. GlnN, GlnO, AsnN and AsnO denote N and O atoms in the side chains of Gln63 and Asn45, respectively.

ca 1.6 nm in both the Y21F and W104F AppAs, which was much longer than those between Iso and Trp104 or Tyr21. The mean inter-ring angle between Iso and Trp104 or Tyr21 in both Y21F and W104F was remarkably different from that in the WT AppA (Table 1).

3.2. H bond dynamics and distance distribution around Iso in mutated AppA

The H bond dynamics of the WT AppA were first obtained by Obanayama et al. [59], and our previous work [45]. Here, the H bond distance distribution between the potential proton donor and the acceptors in the Y21F and W104F mutant AppAs are shown in Fig. 3, whilst the time-dependent changes in these H bond distances are shown in Figs. S1 and S2 (Supplementary information), with the mean H bond distances summarized in Table 2. The distribution of the H bond distances between the IsoO4/Gln63N pair in Y21F is quite broad, suggesting a marked fluctuation in the distance. The time-dependent changes in the distance of the Trp104NH/Gln63O pair in Y21F (see Fig. S1) varied around 0.3 nm, but sometimes increased to more than 0.4 nm after 1.3 ns. Correspondingly, the distribution of the H bond distances for the Trp104NH/Gln63O interaction in the Y21F AppA exhibited a second minor peak at around 0.45 nm which shows two potential minima along the distance. In Y21F, since the H bond between Tyr21OH and Gln63O cannot form, Gln63O mostly forms a H bond with Trp104NH. The most frequent bond length of the Tyr21OH/Gln63O interaction in W104F was 0.28 nm (Fig. 3B), which is very short and so the H bond should be strong, whilst a second minor peak at around 0.38 nm was also seen, which may be ascribed to rotational motion of Gln63, as observed in the WT AppA (discussed later). The distances for the H bonds between IsoO4/Gln63N in Y21F and W104F were broadly and strongly comparable, respectively, to that in the WT AppA, whilst for IsoO4/Asn45N the bond distances in Y21F and W104F were strongly and broadly similar to that in the WT AppA. A H

Table 1The mean distance and angle between Iso and the indicated aromatic amino acids near Iso, as obtained by MD.^a.

System	Distance (nm)				Angle (°)	
	Center-to-center		Edge-to-edge		Trp104	Tyr21
	Trp104	Tyr21	Trp104	Tyr21		
WT ^b	0.887 ± 0.001	0.797 ± 0.0005	0.317 ± 0.001	0.278 ± 0.0006	-60.1 ± 0.17	71.2 ± 0.18
Y21F	0.829 ± 0.001		0.335 ± 0.001		-32.3 ± 0.23	
W104F		0.781 ± 0.0006		0.261 ± 0.0006		93.5 ± 0.36

^a Mean ± S.E.^b Data were taken from Ref. [45] for comparison.**Table 2**The average H bond distances.^a.

AppA	IsoO4/GlnN	IsoO4/AsnN	IsoN3/AsnO	TrpNH/GlnO	TyrOH/GlnO
WT ^b	0.312 ± 0.0005	0.302 ± 0.0004	0.301 ± 0.0005	0.498 ± 0.0021	0.308 ± 0.0018
Y21F	0.347 ± 0.001	0.302 ± 0.0004	0.299 ± 0.0004	0.314 ± 0.001	
W104F	0.313 ± 0.0006	0.362 ± 0.0005	0.302 ± 0.0004		0.278 ± 0.0004

^a Gln, Asn, Trp, and Tyr represent Gln63, Asn45, Trp104 and Tyr21, respectively. Distance ± S.E. was expressed in nm unit. Atomic notations of Iso are shown in Fig. 1.^b Data were taken from Nunthaboot et al. [45].^c Distance of the TrpNH/GlnN pair was 0.38 ± 0.01 nm.

bond chain from Tyr21 to Iso through Gln63 was also formed in the W104F AppA, as in the WT, since the distances of Tyr21OH/Gln63O and Gln63N/IsoO4 were small and very similar between the WT and W104F AppAs (Table 2).

3.3. Rotational transition of Gln63 in WT

The angles between the amide group of Gln63 and Iso, Trp104 and Tyr21 in the WT AppA are shown in Fig. 4, where the angles were around 70° for Iso and Trp104, and around -50° in Tyr21. At around 1 ns a rotational transition was found. The transition occurred from 70° to 110° in Gln63-Iso and -Trp104 interactions, and from -40° to -110° in the Gln63-Tyr21 pairing. The H bond-distance transition of the Tyr21OH/GlnO pair, due to the rotational motion of Gln63, was also found (Fig. S1; Supplementary information), as has been reported before [45]. Similar transitions in the WT AppA displayed in the distances of IsoN5/Gln63O and Trp104NH/Gln63N pairs are consistent with the predicted tautomerization of Gln63 upon excitation of Iso [14]. The present results reveal that the tautomerization of Gln63 can take place in the ground state of Iso without light.

The angles between the Gln63 amide group and the tyrosine in the Y21F and W104 AppAs are shown in Figs. S3 and S4 (Supplementary information), respectively, where in both Y21F and W104F no sudden transition was observed, in contrast to the WT AppA. Fluctuations in the angles were remarkable in Trp104 and Iso in the Y21F AppA but were not so marked in Tyr21 and Iso in the W104F AppA.

3.4. Fluorescence decay analysis by PET theory

Fluorescence decays of the WT [6], Y21F [8] and W104F [9] AppAs were analyzed simultaneously with KM theory and the atomic coordinates obtained by MD. The observed and calculated fluorescence decays, as well as the deviations between these, of the WT, Y21F and W104F AppAs are shown in Fig. 5. Agreement between the calculated and the observed fluorescence decays were very good, with χ^2 values of 4.6×10^{-4} in WT, 3.08×10^{-4} in Y21F, and 1.6×10^{-4} in W104F, with a total χ^2 value of 3.09×10^{-4} . When the WT was analyzed separately, a χ^2 value of 2.86×10^{-6} was obtained [45]. However, when ε_0 , contained in KM theory (Supplementary material A), was held the same among WT, Y21F and W104F, the agreement between the observed and calculated decays was then poor.

3.5. PET parameters

The PET parameters obtained from the simultaneous analyses are listed in Table 3, together with those obtained in the previous work [45]. For the WT AppA, the ratio of ν_0 of Tyr21 to Trp104 was 1.15, which is considerably lower than the previous

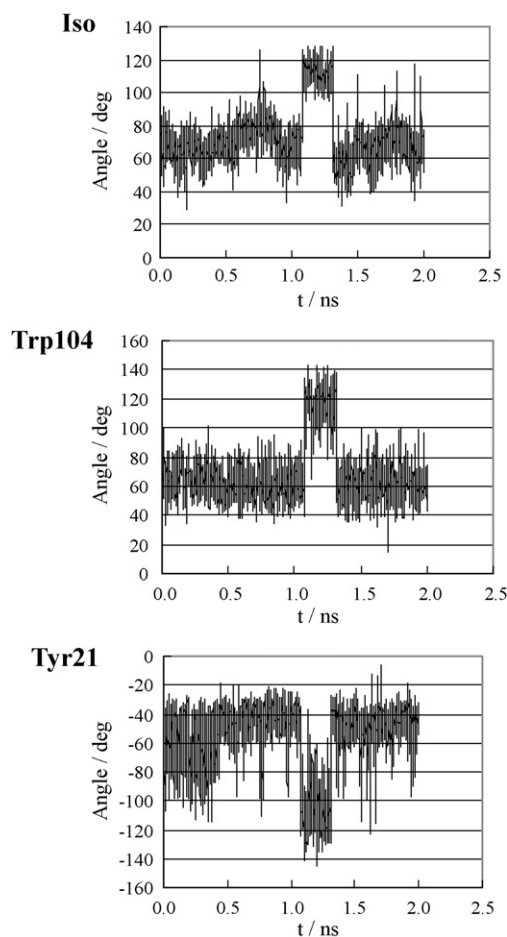


Fig. 4. Inter-planar angle between the amide group of Gln63 and the aromatic rings of the WT AppA. Iso, Trp104 and Tyr21 indicate the inter-planar angles between the amide of Gln63, Trp104 and Tyr21, respectively.

Table 3
PET parameters in KM theory.^a

System	Experimental data [Ref. no.]	PET parameters for Trp104			PET parameters for Tyr21			C_{Iso}^0 (eV)	ε_0	χ^2 ^b
		ν_0 (ps ⁻¹)	β (nm ⁻¹)	R_0 (nm)	ν_0 (ps ⁻¹)	β (nm ⁻¹)	R_0 (nm)			
WT ^c	Gauden et al. ^d [6]	2304	18.1	0.539	2661	6.25	2.74	8.53 ^e	29.0	4.60×10^{-4}
Y21F ^c	Gauden et al. ^f [8]								13.7	3.08×10^{-4}
W104F ^c	Laan et al. ^g [9]								2.45	1.60×10^{-4}
WT	Gauden et al. ^d , [6] Nunthaboot et al. ^h [45]	2228	60.1	0.694	3226	6.25	2.72	8.82 ⁱ	28.9	2.86×10^{-6}

^a KM theory was used for the analyses [40–42].

^b Chi square between the observed and calculated fluorescence intensities, given by Eq. (7).

^c The observed decays of WT, Y21F and W104F were simultaneously analyzed with common PET parameters. The values of ε_0 were defined separately among WT, Y21F and W104F AppAs. The value of total χ^2 was 3.09×10^{-4} .

^d Decay parameters are $\tau_1 = 25$ ps ($\alpha_1 = 0.10$), $\tau_2 = 150$ ps ($\alpha_2 = 0.32$), $\tau_3 = 670$ ps ($\alpha_3 = 0.56$), $\tau_4 = 3.8$ ns ($\alpha_4 = 0.02$).

^e $\Delta G_{\text{Trp}}^0 = 1.33$ eV and $\Delta G_{\text{Tyr}}^0 = 0.533$ eV.

^f Decay parameters are $\tau_1 = 7.5$ ps ($\alpha_1 = 0.170$), $\tau_2 = 55$ ps ($\alpha_2 = 0.42$), $\tau_3 = 212$ ps ($\alpha_3 = 0.40$), $\tau_4 = 7.1$ ns ($\alpha_4 = 0.01$).

^g Decay parameters are $\tau_1 = 47$ ps ($\alpha_1 = 0.14$), $\tau_2 = 555$ ps ($\alpha_2 = 0.63$), $\tau_3 = 2.5$ ns ($\alpha_3 = 0.23$).

^h PET parameters were taken from Ref. [45].

ⁱ $\Delta G_{\text{Trp}}^0 = 1.62$ eV and $\Delta G_{\text{Tyr}}^0 = 0.82$ eV.

report of 1.45 for WT AppA [45], but still much higher than that in a non-photosensing flavoprotein of FBP (0.194) [44]. The high value of ν_0 in Tyr21 was elucidated in terms of H bond effect in Iso*–Gln63–Tyr21 system [45]. In the present work, ε_0 , in Eqs. (A1) and (A2) in Supplementary material A, was defined separately among the three forms of AppA, with ε_0 values of that were 2.1- and 11.8-fold higher in the WT than in Y21F and W104F, respectively (Table 3). The high dipole moments of Trp104 or Tyr21 may contribute to the ε_0 values, together with the presence of water molecules around Iso in the WT. The dipole moment of Trp104 in Y21F, or Tyr21 in W104F, becomes almost zero in these two AppAs, which may be one of the reasons why their ε_0 values are lower than that in the WT. The derived value for ε_0 in the WT AppA was quite close to that reported previously (20–28.9) [45]. The values of β in Trp104 and Tyr21 were 1.3-fold higher and 2.2-fold lower, respectively, than that in other photosynthetic systems (14) [36]. However, the values of β in the other reported photosynthetic systems was obtained with edge-to-edge donor–acceptor distances, while in this work the distances were obtained as center-to-center distances [26]. R_0 represents the threshold distance between the adiabatic and non-adiabatic processes of PET. The values of R_0 obtained in this study for the WT AppA for Trp104 and Tyr21 were similar and the same, respectively, to those reported in previous work (0.694 and 2.74 nm, respectively) [45]. It is not clear whether the R_0 value of 2.7 nm for Tyr21 is correct or not, but at least it is much larger than the R_0 in the Iso*–Trp104 system or in the FMN binding protein. The very large value of R_0 in the Iso*–Tyr21 system may be ascribed to the H bond chain between Iso* and Tyr21 through Gln63.

3.6. PET rate and electrostatic energy

The PET rates were obtained using the best-fit PET parameters listed in Table 3, and are shown in Fig. 6. The mean PET rates were 0.0215 ($1/46.5$ ps) ± 0.00024 ps⁻¹ from Trp104 to Iso* in Y21F, and 0.00309 ($1/324$ ps) ± 0.00005 ps⁻¹ from Tyr21 to Iso* in W104F. In the present analysis, the PET rate was seven times faster from Trp104 to Iso* in Y21F than from Tyr21 to Iso* in W104F. In comparison, the PET rates for the WT AppA were 0.001175 ps⁻¹ ($1/851$ ps) from Trp104 to Iso* and 0.00099 ps⁻¹ ($1/1010$ ps) from Tyr21 to Iso* in WT [45].

The time-dependent changes in the electrostatic energy in Y21F are shown in Fig. S6 (Supplementary information), where the mean energies were 0.36 eV for the Iso anion and -0.23 eV for the Trp104 cation.

3.7. Charge density and interaction energy in Iso*–Trp104–Tyr21–Gln63 system of WT

The time-dependent changes in charge densities at Iso*, Trp104, Tyr21 and Gln63 are shown in Fig. 7A. The initial structures were constructed from MD structures at every 50 ps interval up to 2 ns. Iso was substituted by lumiflavin, Trp by 3-methylindole, Tyr by p-cresol and Gln by propanamide. These structures were geometrically optimized using the PM3 method. Total charge densities at Trp104 were 0.947 at 0.4 ns, 0.855 at 0.8 ns and 0.892 at 1.85 ns, whilst those at Iso* were -0.943 at 0.4 ns, -0.88 at 0.8 ns, and -0.869 at 1.85 ns. Thus the positive charge densities at Trp104 were well correlated with the negative charge densities at Iso*. The dipole moment of the Iso*–Trp104–Tyr21–Gln63 system is shown in Fig. S7, where the charge densities at Tyr21 and Gln63 were very low.

The interaction energies among Iso*, Trp104, Tyr21 and Gln63 were calculated by Eq. (11), and are shown in Fig. 7B. The energy displayed a clear oscillatory behavior with time, which is similar to the changes in the charge densities. The correlation between the interaction energy and charge densities at Iso* and Trp104 is shown in Fig. 8. As the absolute value of the energy decreased, the charge densities at both Iso* and Trp104 were reduced. The charge densities at Iso* and Trp104 were minimal and maximal, respectively, at an interaction energy of around -20 (kcal/mol). As the absolute values of the interaction energy became greater than -20 (kcal/mol), the transferred charge again tended to decrease. In the WT AppA, Iso*–Trp104–Gln63 interaction (see Fig. S8) and in FBP [58], such a relationship was not clear since the calculation systems of these studies were rather small compared to the present work.

4. Discussion

In the present work, the theoretical basis for PET in AppA was driven from the fluorescence dynamics of WT, Y21F and W104F, using PET theory. Fluorescence decay in the PET systems of WT, Y21F and W104F were satisfactorily reproduced with KM theory and MD atomic coordinates. PET parameters contained in KM theory were similar with those reported in previous work (see Table 3), which were obtained by analyzing the fluorescence decay of the WT AppA alone. In previous works [44,58], we have shown that; (1) the interaction energy (Y) was expressed as a 3rd order polynomial of X [$\ln(\text{PET rate in ps}^{-1} \text{ unit})$], $Y = 0.0036X^3 + 0.0306X^2 - 1.7822X - 21.177$, (2) the photoinduced charge transfer (charge transfer obtained by MO) takes place only when the interaction energy is great, but that the opposite is not

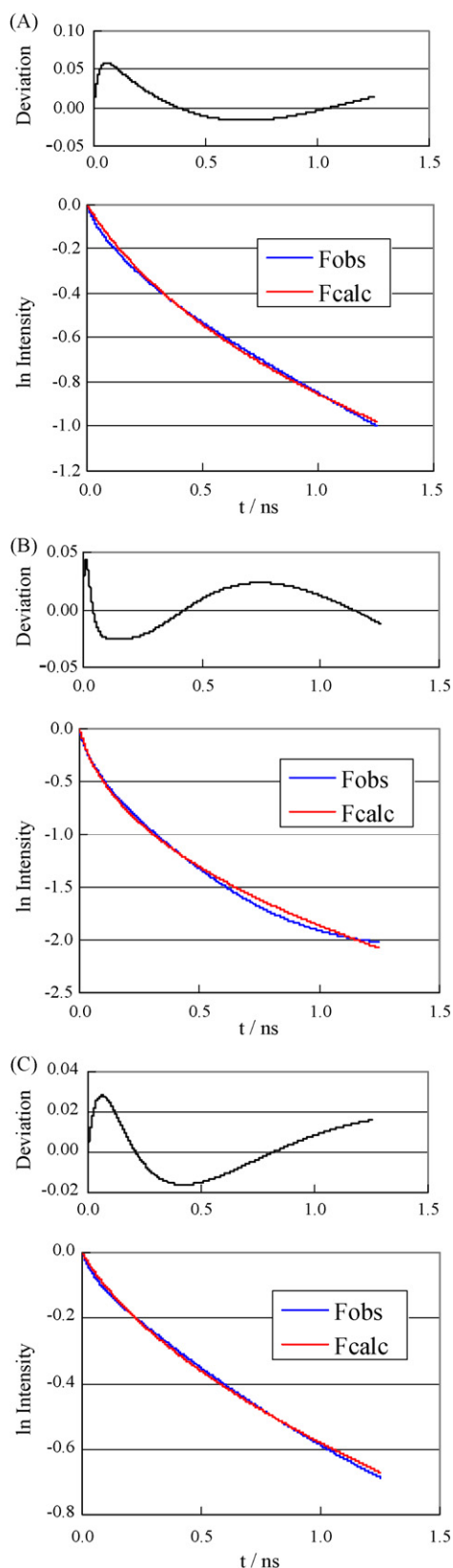


Fig. 5. The observed (Fobs) and calculated (Fcalc) fluorescence decays obtained by the simultaneous analyses of (A) WT, (B) Y21F and (C) W104F. Fcalc was obtained with KM theory and MD structures. The best-fit PET parameters contained in the KM theory were determined according to the non-linear least squares method, as described in text (see Table 3). The observed decays of WT, Y21F and W104F were from [6,8,9], respectively. The upper panel of each fluorescence decay shows the deviation between the observed and calculated decays. The values of χ^2 were 4.60×10^{-4} in WT, 3.08×10^{-4} in Y21F, and 1.60×10^{-4} in W104F.

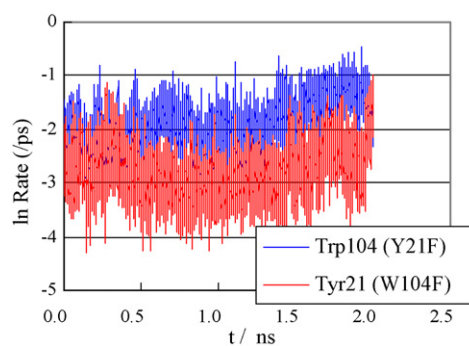


Fig. 6. PET rates from the aromatic amino acids to Iso* obtained with PET parameters determined by the simultaneous analyses of WT, Y21F and W104F. Trp104 (Y21F) denotes the PET rate from Trp104 to Iso* in Y21F and Tyr21 (W104F) that from Tyr21 to Iso* in W104F. PET parameters used for the calculation are listed in Table 3.

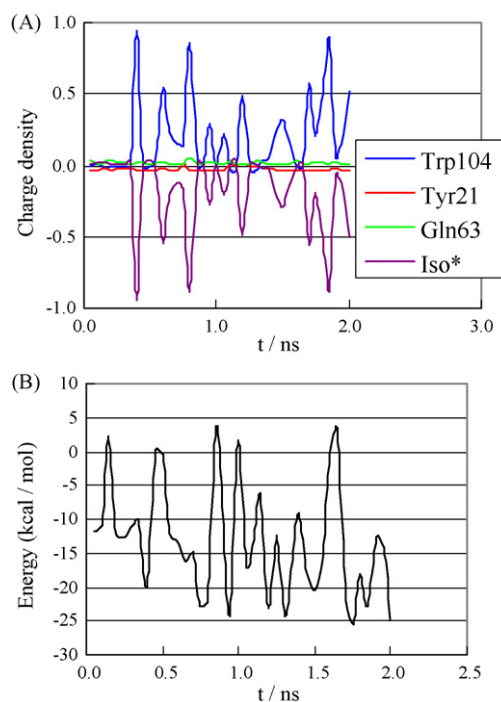


Fig. 7. Time-dependent changes in the charge density and interaction energy in the Iso*–Trp104–Tyr21–Gln63 system. (A) Total charge densities of Trp104, Tyr21, Gln63 and Iso*. (B) Interaction energy. Iso, Trp, Tyr and Gln were substituted with lumiflavin, 3-methylindol, p-cresol and propanamide, respectively. Initial configurations of these compounds were constructed from MD structures at 50 ps time intervals up to 2 ns. The charge densities and the interaction energies were obtained by the PM3 method, according to Eq. (11) in text.

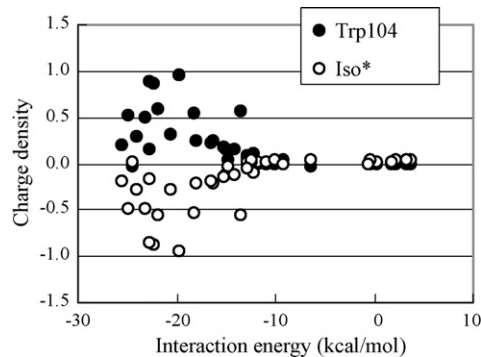


Fig. 8. Correlation between the interaction energy and charge density in Iso*–Trp104–Tyr21–Gln63 system. Trp104 and Iso* indicate charge densities at Trp104 and Iso*, respectively.

true, namely, sometimes photoinduced charge transfer does not take place even though the interaction energy is great, and (3) the ν_0 of Trp as a donor is much greater than that of Tyr, which correlates very well with the much higher PET rate from Trp than from Tyr in the FMN binding protein.

In this work the value of ν_0 of Tyr21 in AppA was much greater than that reported for the non photosensing protein of FBP [44], which is in accordance with a previous report [45], and that ν_0 is related to the electronic interaction energy between the electron donor and acceptor. The value of R_0 in the Iso*–Tyr21 interaction was also much longer than that in the Iso*–Trp104 interaction. When the donor–acceptor distance is shorter than R_0 , the electronic interaction is high and so PET process becomes adiabatic. The very large R_0 value in the Iso*–Tyr21 interaction suggests that the electronic interaction energy is quite large at $R < R_0$, which may also be elucidated from the H bond chain between Iso and Tyr21 through Gln63. Certainly, the high interaction energy between Iso* and Tyr21 was ascribed to the H bond chain between Tyr21 and Iso* through Gln63, and verified by a non-empirical MO method [14]. Such fast PET through H bonding between an aromatic electron donor and acceptor has also been observed previously in organic compounds by means of transient absorption spectroscopy [46–49].

Using the X-ray structure obtained by Jung et al. [12], as the initial structure for the dark state, Domratcheva et al. [14] proposed that upon excitation Gln63 undergoes a tautomerization with H bond switching from Tyr21OH/Gln63O:GlnNH/IsoN5 to Tyr21OH/Gln63NH:GlnO/Iso*5H. In this model Trp104 is distant from Iso (Trp_{out}), with a center-to-center distance of 1.47 nm according to the X-ray structure [12]. At this distance, PET from Trp104 to Iso* is unlikely to take place in the sub-nanosecond time domain [26,27]. However, in marked contrast, fluorescence dynamics experiments revealed that the PET rate in Y21F AppA does not differ much from that of the WT [6,8,9], which implies that the distance between Iso and Trp104 is likely to be much shorter than 1.47 nm, as given by Anderson et al. [4].

The PM3 MO method was able to elucidate PET from Trp to Iso* in both FBP [58] and WT AppA [45], but not from Tyr to Iso* in the WT AppA [45]. In the present work, we have obtained the interaction energy in the system of Iso*–Trp104–Tyr21–Gln63. Charge transfer mainly took place from Trp104 to Iso*, even though all the components related to PET in BLUF of AppA were taken into account. PET from Tyr21 to Iso* could not be explained by the PM3 method. The interaction energy correlated well with amount of transferred charge from Trp104 to Iso*. It is of interest that the transferred charge from Trp to Iso* was maximal at the interaction energy of around –20 kcal/mol, and the transfer charge was reduced as the absolute value of the interaction energies increased.

Acknowledgements

This work was supported by the annual government statement of expenditure of Mahasarakham University (fiscal year 2010). We would like to acknowledge the Computational Chemistry Unit Cell, Chulalongkorn University, for use of the computing facilities. The Center of Excellence for Petroleum, Petrochemicals, and Advanced Materials, Chulalongkorn University, is acknowledged.

Appendix A. Supplementary data

Supplementary data associated with this article can be found, in the online version, at doi:10.1016/j.jphotochem.2009.10.013.

References

[1] S. Masuda, C.E. Bauer, *Cell* 110 (2002) 613–623.

- [2] B.J. Kraft, S. Masuda, J. Kikuchi, V. Dragnea, G. Tollin, J.M. Zaleski, C.E. Bauer, *Biochemistry* 42 (2003) 6726–6734.
- [3] O.V. Moskvina, S. Kaplan, M.-A. Gilles-Gonzalez, M. Gomelsky, *J. Biol. Chem.* 282 (2007) 28740–28748.
- [4] W. Laan, M.A. van der Horst, I.H.M. van Stokkum, K.J. Hellingwerf, *Photochem. Photobiol.* 78 (2003) 290–297.
- [5] S. Anderson, V. Dragnea, S. Masuda, J. Ybe, K. Moffat, C.E. Bauer, *Biochemistry* 44 (2005) 7998–8005.
- [6] S. Masuda, K. Hasegawa, T. Ono, *Biochemistry* 44 (2005) 1215–1224.
- [7] M. Gauden, S. Yeremenko, W. Laan, I.H.M. van Stokkum, J.A. Ihalainen, R. van Grondelle, K.J. Hellingwerf, J.T.M. Kennis, *Biochemistry* 44 (2005) 3653–3662.
- [8] V. Dragnea, M. Waegle, S. Balascuta, C. Bauer, B. Dragnea, *Biochemistry* 44 (2005) 15978–15985.
- [9] M. Gauden, J.S. Grinstead, W. Laan, I.H.M. van Stokkum, M. Avila-Perez, K.C. Toh, R. Boelens, R. Kaptein, R. van Grondelle, K.J. Hellingwerf, J.T.M. Kennis, *Biochemistry* 46 (2007) 7405–7415.
- [10] W. Laan, M. Gauden, S. Yeremenko, R. van Grondelle, J.T.M. Kennis, K.J. Hellingwerf, *Biochemistry* 45 (2006) 51–60.
- [11] M. Gauden, I.H.M. van Stokkum, J.M. Key, D.C. Lührs, R. van Grondelle, P. Hegemann, J.T.M. Kennis, *Proc. Nat. Acad. Sci. U.S.A.* 103 (2006) 10895–10900.
- [12] A. Jung, J. Reinstein, T. Domratcheva, R.L. Shoeman, I. Schlichting, *J. Mol. Biol.* 362 (2006) 717–732.
- [13] K.C. Toh, I.H.M. van Stokkum, J. Hendriks, M.T.A. Alexandre, J.C. Arents, *Biophys. J.* 95 (2008) 312–321.
- [14] T. Domratcheva, B.L. Grigorenko, I. Schlichting, A.V. Memukhin, *Biophys. J.* 94 (2008) 3872–3879.
- [15] S. Masuda, K. Hasegawa, T. Ono, *Biochemistry* 43 (2004) 5304–5313.
- [16] H. Yuan, S. Anderson, S. Masuda, Y. Dragnea, K. Moffat, C.E. Bauer, *Biochemistry* 45 (2006) 12687–12694.
- [17] R. Takahashi, K. Okajima, H. Suzuki, H. Nakamura, M. Ikeuchi, T. Noguchi, *Biochemistry* 46 (2007) 6459–6467.
- [18] C. Bonetti, T. Mathes, I.H.M. van Stokkum, K.M. Mullen, M.-L. Groot, R. van Grondelle, P. Hegemann, J.T.M. Kennis, *Biophys. J.* 95 (2008) 4790–4802.
- [19] Q. Wu, W.-H. Ko, K.H. Gardner, *Biochemistry* 47 (2009) 10271–10280.
- [20] H. Nagai, Y. Fukushima, K. Okajima, M. Ikeuchi, H. Mino, *Biochemistry* 47 (2009) 12574–12582.
- [21] Y. Fukushima, Y. Murai, K. Okajima, M. Ikeuchi, S. Itoh, *Biochemistry* 47 (2009) 660–669.
- [22] N. Mataga, H. Chosrowjan, Y. Shibata, F. Tanaka, *J. Phys. Chem. B* 102 (1998) 7081–7084 (Letter).
- [23] N. Mataga, H. Chosrowjan, Y. Shibata, F. Tanaka, Y. Nishina, K. Shiga, *J. Phys. Chem. B* 104 (2000) 10667–10677.
- [24] N. Mataga, H. Chosrowjan, S. Taniguchi, F. Tanaka, N. Kido, M. Kitamura, *J. Phys. Chem. B* 106 (2002) 8917–8920 (Letter).
- [25] F. Tanaka, N. Mataga, *Trends Chem. Phys.* 11 (2004) 59–74.
- [26] F. Tanaka, H. Chosrowjan, S. Taniguchi, N. Mataga, K. Sato, Y. Nishina, K. Shiga, *J. Phys. Chem. B* 111 (2007) 5694–5699.
- [27] F. Tanaka, R. Rujkorakarn, H. Chosrowjan, S. Taniguchi, N. Mataga, *Chem. Phys.* 348 (2007) 237–241.
- [28] H. Chosrowjan, S. Taniguchi, N. Mataga, F. Tanaka, D. Todoroki, M. Kitamura, *J. Phys. Chem. B* 111 (2007) 8695–8697 (Letter).
- [29] H. Chosrowjan, S. Taniguchi, N. Mataga, F. Tanaka, D. Todoroki, M. Kitamura, *Chem. Phys. Lett.* 462 (2008) 121–124.
- [30] A. Karen, N. Ikeda, N. Mataga, F. Tanaka, *Photochem. Photobiol.* 37 (1983) 495–502.
- [31] A. Karen, M.T. Sawada, F. Tanaka, N. Mataga, *Photochem. Photobiol.* 45 (1987) 49–53.
- [32] D. Zhong, A. Zewail, *Proc. Natl. Acad. Sci. U.S.A.* 98 (2001) 11867–11872.
- [33] J. Pan, M. Byrdin, C. Aubert, A.P.M. Eker, K. Brettel, M.H. Vos, *J. Phys. Chem. B* 108 (2004) 10160–10167.
- [34] R. Marcus, *J. Chem. Phys.* 24 (1956) 979–989.
- [35] R. Marcus, N. Sutin, *Biochim. Biophys. Acta* 811 (1985) 265–322.
- [36] C. Moser, J. Keske, K. Warncke, R. Farid, P. Dutton, *Nature* 355 (1992) 796–802.
- [37] M. Bixon, J. Jortner, *J. Phys. Chem.* 95 (1991) 1941–1944.
- [38] M. Bixon, J. Jortner, *J. Phys. Chem.* 97 (1993) 13061–13066.
- [39] M. Bixon, J. Jortner, J. Cortes, H. Heitele, M.E. Michel-Beyerle, *J. Phys. Chem.* 98 (1994) 7289–7299.
- [40] T. Kakitani, N. Mataga, *J. Phys. Chem.* 89 (1985) 8–10.
- [41] T. Kakitani, A. Yoshimori, N. Mataga, *J. Phys. Chem.* 96 (1992) 5385–5392.
- [42] T. Kakitani, N. Matsuda, A. Yoshimori, N. Mataga, *Prog. React. Kinet.* 20 (1995) 347–381.
- [43] N. Nunthaboot, F. Tanaka, S. Kokpul, H. Chosrowjan, S. Taniguchi, N. Mataga, *J. Photochem. Photobiol. A: Chem.* 201 (2009) 191–196.
- [44] N. Nunthaboot, F. Tanaka, S. Kokpul, H. Chosrowjan, S. Taniguchi, N. Mataga, *J. Phys. Chem. B* 112 (2008) 13121–13127.
- [45] N. Nunthaboot, F. Tanaka, S. Kokpul, *J. Photochem. Photobiol. A* 207 (2009) 274–281.
- [46] N. Mataga, Y. Kaifu, M. Koizumi, *Naturwissenschaften* 44 (1956) 304–310.
- [47] N. Mataga, F. Tanaka, K. Kato, *Acta Phys. Polon.* 34 (1968) 733–745.
- [48] N. Ikeda, H. Miyasaka, T. Okada, N. Mataga, *J. Am. Chem. Soc.* 105 (1983) 5206–5220.
- [49] H. Miyasaka, A. Tabata, S. Ojima, N. Ikeda, N. Mataga, *J. Phys. Chem.* 97 (1993) 8222–8227.
- [50] N. Guex, M.C. Peitsch, *Electrophoresis* 18 (1997) 2714–2723.

- [51] D. Case, T. Darden, T. Cheatham, C. Simmerling, J. Wang, R. Duke, R. Luo, K. Merz, B. Wang, D. Pearlman, M. Crowley, S. Brozell, V. Tsui, H. Gohlke, J. Mongan, V. Hornak, G. Cui, P. Beroza, C. Schafmeister, J. Caldwell, W. Ross, P. Kollman, AMBER 8, University of California, San Francisco, 2004.
- [52] J.M. Wang, P. Cieplak, P.A. Kollman, *J. Comp. Chem.* 21 (2000) 1049–1074.
- [53] C. Schneider, J. Suhnel, *Biopolymers* 50 (1999) 287–302.
- [54] U. Essmann, L. Perera, M.L. Berkowitz, T. Darden, H. Lee, G. Pedersen, *J. Chem. Phys.* 103 (1995) 8577–8593.
- [55] J.-P. Ryckaert, G. Cicotti, H.J.C. Berendsen, *J. Comp. Phys.* 23 (1977) 327–341.
- [56] V. Vorsa, T. Kono, K.F. Willey, L. Winograd, *J. Phys. Chem. B* 103 (1999) 7889–7895.
- [57] E.R. Henry, R.M. Hochstrasser, *Proc. Natl. Acad. Sci. U.S.A.* 84 (1987) 6142–6146.
- [58] N. Nunthaboot, F. Tanaka, S. Kokpol, H. Chosrowjan, S. Taniguchi, N. Mataga, *J. Phys. Chem. B* 112 (2008) 15837–15843.
- [59] K. Obayama, H. Kobayashi, K. Fukushima, M. Sakurai, *Photochem. Photobiol.* 84 (2008) 1003–1010.